■原著論文／ORIGINAL PAPER ■

Shock-Tube and Modeling Study of Dimethyl Ether Pyrolysis and Oxidation

WAKAMATSU, Hitoshi, ISHIHARA, Akiko, HOSHIKAWA, Hiroshi, SATOH, Kazutaka, YAMANE, Masatsugu, and HIDAKA, Yoshiaki*

Department of Chemistry, Faculty of Science, Ehime University, Bunkyo-cho, Matsuyama 790-8577, Japan

Abstract : Pyrolysis and oxidation in fuel-rich and fuel-lean mixtures of dimethyl ether (DME) highly diluted with argon were studied behind reflected shock waves in the temperature range 950 - 1900 K at total pressures between 0.8 and 2.9 atm. The study was carried out using the following methods: 1) time-resolved IR-laser absorption at 3.39 μm for DME decay and CH-compound formation rates, 2) time-resolved UV absorption at 216 nm for the CH_3 radical formation rate, 3) time-resolved UV absorption at 306.7 nm for the OH radical formation rate, 4) time-resolved IR emission at 4.24 μm for the CO_2 formation rate, and 5) a single-pulse technique for product yields. The pyrolysis and oxidation of DME, which were for very wide mixture compositions ranging from highly DME-rich to highly DME-lean, were modeled using a reaction mechanism with 178 reaction steps and 53 species including the most recent sub-mechanisms for formaldehyde, ketene, methane, acetylene, and ethylene oxidation. This and previously reported data were reproduced using this mechanism. The rate constant $k_5 = 4.5 \times 10^{14} \exp(- 6.1 \text{ kcal/RT}) \text{ cm}^3\text{mol}^{-1}\text{s}^{-1}$ of reaction DME + OH → CH_3OCH_2 + H_2O was evaluated.

Key Words : Shock tube, Modeling; Dimethyl ether, Pyrolysis, Oxidation

1. Introduction

Due to a high cetane number and low soot formation, dimethyl ether (DME) has been proposed as an alternative diesel fuel. A test using DME as the fuel for diesel engines has been carried out. The kinetics of DME oxidation has been studied in the temperature range 800 - 1300 K by several groups [1-4]. Dagaut et al. [1] have studied DME oxidation using a jet-stirred reactor under a wide range of conditions: 1 - 10 atm and 800 - 1300 K. They measured concentration profiles of reactant, intermediates, and products of DME oxidation by probe sampling and GC analyses and proposed a detailed reaction mechanism with 286 reactions. Dagaut et al. [2] have also studied concentration profiles at lower temperature of 550 - 1100 K using a jet-stirred reactor and an ignition delay in the temperature range 1200 - 1600 K using a shock tube, and reported an updated version of DME oxidation mechanism that they developed earlier [1]. Curran et al. [3] have proposed a detailed chemical model reproducing the reported results obtained in both the jet-stirred reactor [1] and a shock tube [5]: the numerical model consisted of 78 chemical species and 336 chemical reactions. More recently, Fischer et al. [4] developed a new DME

oxidation mechanism from data obtained with two different flow reactors, (1) a variable-pressure flow reactor at 2.5 atm and 1118 K, and (2) an atmospheric pressure flow reactor at about 1085 K; the mechanism consisted of 82 chemical species and 351 chemical reactions. The DME oxidation mechanism and the rate constant expressions are now fairly clear.

The mechanism of DME pyrolysis is an essential part of the oxidation mechanism. It is useful to study the DME pyrolysis and oxidation mechanisms together. However, no combined modeling study has been carried out for the DME pyrolysis and oxidation at temperatures above 1300 K. Also, there is no report on DME oxidation in highly fuel-rich and fuel-lean mixtures above 1300 K. The only data reported above 1300 K were observed with mixtures of equivalence ratios 0.5 $\leq \Phi \leq$ 2 and were obtained by observing light emission at 366 nm for carbon dioxide chemiluminescence in the temperature range 1200 - 1600 K using the shock tube [2].

In the present paper, we report results from a study of DME pyrolysis and DME oxidation in highly fuel-rich and fuel-lean mixtures in the temperature range 950 - 1900 K at pressures in the range 0.8 - 2.9 atm using a shock tube technique. We propose a detailed reaction mechanism to reproduce wide mixture compositions ranging from DME-rich (including DME pyrolysis) to DME-lean.

* Corresponding author. E-mail: hidaka@dpc.ehime-u.ac.jp

2. Experimental

Three different shock tubes of 4.1 cm i.d. were used in this study. The first shock tube was a magic-hole-type, which had the facility for both single-pulse and time-resolved spectroscopy. Only a simple description of this shock tube is given below since the apparatus has been described in detail previously [6-9]. The reacted gases quenched by the single-pulse method were extracted into a pre-evacuated vessel (50 cc) through a valve located at the distance of 1 cm from the end plate. The reacted mixture was analyzed by three serially connected gas chromatographs, each having a thermal-conductivity detector. The gas-chromatographic analysis, which was similar to that used previously [7,8], was used to determine the concentrations of reactant and products. The reactant and product mole fractions were determined within an accuracy of ± 4 %. An effective heating time t_e (reaction time), which was defined as the time between the arrival of the reflected shock wave and the 80 % point of fall from the initial reflected shock pressure, was determined with an accuracy of ± 5 % using the method previously described [6,7]. The relationship between t_e and temperature showed that the t_e increased with a decrease in temperature, as seen in Fig. 2 of Ref. 6. Hence, the t_e values at representative temperatures were evaluated from the relationship between the observed t_e and temperature. The t_e values are shown in each of the figure captions. Assuming that the reaction was frozen at the effective heating time t_e, the concentrations of carbon-containing compounds, determined by gas chromatography, were compared with those from the simulation.

The second shock tube was a standard-type shock tube connected to a laser absorption and IR emission equipment [10,11]. The window was located at the same distance of 1 cm from the reflected shock plate as the laser-beam window. The transmitted intensity of a 3.39 μm He-Ne laser beam through a 4.1 cm path-length in the shock tube and through an interference filter (λ_{max} = 3.39 μm, halfwidth = 0.072 μm) was monitored with an InSb detector using the same method as used previously [10,11]. The 3.39 μm laser beam was absorbed by many CH compounds, but mainly by DME, C_2H_6, C_2H_4, and CH_4 under our experimental conditions. The extinction coefficients for the reactant and products were measured previously [10-12]. The equations relating the extinction coefficient of each species to the measured temperature were used in the simulations reported here. In this experiment, an IR emission technique similar to that used previously [8] was used to monitor the formation of CO_2. The IR emission was observed with a Hamamatsu P-5968-200 InSb detector through a CaF_2 window, an interference

filter λ_{max} = 4.24 μm, halfwidth = 0.1 μm, and two 0.8-mm slits at each end of a 2-cm-long cylindrical tube. The relative emission at 4.24 μm comes not only from CO_2, but also from CH_2CO and CO under our experimental conditions. The relative emission intensity of these compounds against temperature was measured and shown in Ref. 9. These equations were used in the simulations reported here.

The third shock tube was a standard-type device connected to a UV absorption equipment similar to that previously reported [7,9,11] and an IR-emission equipment. The IR-emission window was located at the same distance of 1 cm from the reflected shock plate as the UV absorption window. The transmitted intensity at 216 nm of a D_2-lamp through a 4.1 cm path-length in the shock tube, dispersed by a grating monochromator, was monitored with a photomultiplier, by the same method used previously [11]. In order to observe the OH radical profile, light at 306.7 nm from a microwave discharge of H_2O in He was also used as a light source instead of the D_2-lamp. The IR-emission of 4.24 μm was observed with a Hamamatsu P-5968-200 InSb detector through a CaF_2 window, an interference filter (λ_{max} = 4.24 μm, halfwidth = 0.1 μm) and two 0.8-mm slits at each end of a 2-cm-long cylindrical tube.

Gas mixtures were prepared manometrically. The composition of reactant mixtures employed is shown in Table 1. The uncertainty in mole fraction of DME, hydrogen and oxygen fraction was less than ± 0.02 %. The initial pressure (P_1) of the used gas mixtures (reactants) was (50 ± 0.1) Torr. The argon (Teisan Co.), H_2 (Chuunenfaiingasu Co.) and O_2 (Seitetsu Kagaku Co.) specified to be 99.999 %, 99.99 %, and 99.995 % pure, respectively, were used without further purification. The DME (Tokyo Kasei Kogyo Co.), specified to be 99 % pure, was frozen and purified by trap-to-trap distillation before use. All shock temperatures and pressures

Table 1. Test Gas Mixtures Used

Mixture	CH3OCH3 (%)	H2 (%)	O2 (%)	Ar (%)
A1	4.0			96.0
A2	2.0			98.0
A3	1.0			99.0
A4	0.2			99.8
A5	4.0		2.0	94.0
A6	2.0		3.0	95.0
A7	2.0		1.0	97.0
A8	1.0		3.0	96.0
A9	1.0		6.0	93.0
A10	1.0		30.0	69.0
A11	0.2		0.6	99.2
A12	0.2		6.0	93.8
A13	0.1	1.0	1.0	97.9

were calculated from the measured incident shock velocity assuming full vibrational relaxation but no chemical reaction. The incident shock velocity was measured with three equally spaced pressure transducers mounted along the end portion of the shock tube. The pressure transducer, which was the nearest to the end wall, was located at 1 cm from that of the shock tube. The incident shock velocity that extrapolated to the end wall was used in the calculations of the temperature T_5. These temperatures and pressures were used for all Figures and Tables. The uncertainty in the calculated temperatures is estimated to be ± 1.2 %.

The computer simulation done in this study was essentially the same as previously described [7-17]. The computer routine used in the simulations was a Gear-type integration of a set of differential equations describing the chemical kinetics under constant density conditions for a reflected shock wave. Reverse reactions were automatically included in the computation through equilibrium constants calculated from thermochemical data. Under our experimental conditions, temperatures in the reaction zone changed with reaction progress; hence the temperature change must be considered in calculating the concentration-time variations and the emission or absorption intensity-time variations of a species. The computer program contained the expressions relating the temperature change to the reaction progress. The computations were carried out by changing the rate-constant value for each elementary reaction every 0.001 K. The time variations of emission or absorption intensity were also calculated considering both the concentration change and the dependence of the emission or absorption intensity on temperature. The above equations of the emission or absorption intensity of each species and temperature were used for these computations.

The basic thermochemical source was the JANAF table [18]. Thermochemical data for HO_2 was taken from GRI 3.0 [19]. Thermochemical data adopted from other than the JANAF tables and [20] were shown in Table 2 of [8, 12].

3. Results

3.1. Intermediate Product Distribution

The stable intermediate product distributions for mixtures A2, A3, and A7 were determined in the temperature range 950 - 1700 K by analyzing the concentrations by the gas chromatograph. These experimental results except mixture A7 were shown in Ref. 20. The intermediate product distribution for mixture A7 is shown in Fig. 1a. The experimental errors of the concentrations are less than ± 2 %. Under our experimental conditions, the main stable products detected by the gas chromatograph were H_2, CO, CH_4, C_2H_4,

and C_2H_2. The species C_3H_6, AC_3H_4 (allene), C_3H_4 (propyne), C_4H_4 (vinylacetylene), 1,3-C_4H_6 were not detected under our experimental conditions. At the same temperature, the yields of C_2H_4, C_2H_2, and DME in mixture A2 were almost the same as those in mixture A3. However, the yield of CH_4 in mixture A2 was about 8 % larger than in mixture A3. It was found that the use of higher DME concentrations resulted in an increase in CH_4 yield. Mixture A7 including O_2 produced CO_2 in addition to the products of the DME pyrolysis.

3.2. Time-resolved IR-laser Absorption at 3.39 μm

To determine time-resolved CH compound concentrations in DME pyrolysis or oxidation, the IR laser absorption at 3.39 μm was measured. The measured absorption profiles were used to estimate concentration profiles of DME and product species. Three typical absorption profiles in DME oxidation with mixtures A5, A6, A8, and A9 are shown in Figs. 2a, 3a, 4a, and 5. Three or four typical absorption profiles in DME pyrolysis with mixtures A1 and A4 were shown in Figs. 1a and 4a of Ref. 20. At temperatures below 1100 K, the absorption intensities after the rapid rise at the reflected shock front remained constant for about 1000 μs. At temperatures above 1100 K, the absorption intensities after the rapid rise slowly decreased with time. A_t is defined by the following equation:

$$A_t = \log (I_f/I_t) / \log (I_f/I_0),$$

where I_f is the signal voltage corresponding to the full intensity and I_0 and I_t are the signal voltages corresponding to the absorption intensity at the reflected shock front (t = 0) and at time t, respectively. The relationship between the extinction coefficient and temperature T was calculated from the observed reflected shock absorption profiles. The equation for the extinction coefficient obtained for DME using mixtures A1, A2, A4, and A5 was I_a (DME) = 6.06 x 10^4 - 13.2 x T cm^2mol^{-1}. Also, in order to determine the simulated A_t of each product at 3.39 μm, the extinction coefficients were measured using mixtures, 2 % C_2H_6, 6 % C_2H_4, 6 % C_2H_2, and 5 % CH_4, respectively, diluted with Ar. The equations for the extinction coefficients obtained for these species were, I_a (C_2H_6) = 5.43 x 10^4 - 17.5 x T cm^2mol^{-1}, I_a (C_2H_4) = 3.38 x T cm^2mol^{-1}, I_a (C_2H_2) = - 1.44 x 10^3 + 1.03 x T cm^2mol^{-1}, I_a (CH_4) = 3.46 x 10^4 - 16.7 x T cm^2mol^{-1} (T < 1500 K) or I_a (CH_4) = 1.18 x 10^4 - 2.51 x T cm^2mol^{-1} (T > 1500 K), respectively. These were determined within an accuracy of ± 5 %. These equations were used in the simulations calculated here.
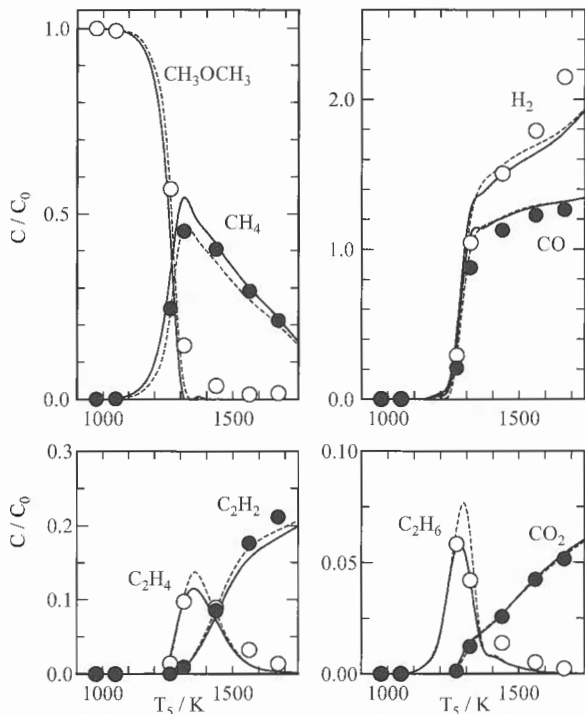
Fig. 1a. Product distribution measured with mixture A7. C_0 is the initial concentration of DME, and C is the concentration of reactant or products at the effective heating time t_e at temperature T and P_1 = 50 Torr. The total pressure and density ranges used are 0.9 - 2.7 atm and 1.2×10^{-5} - 2.0×10^{-5} mol/cm^3, respectively. The t_e values obtained at representative temperatures, 900 K, 1000 K, 1100 K, 1200 K, 1300 K, 1400 K, 1500 K, 1600 K, and 1700 K were 2000 μs, 1970 μs, 1930 μs, 1890 μs, 1860 μs, 1820 μs, 1780 μs, 1750 μs and 1710 μs, respectively. ○, ●, observed; ———, calculated using DMEH-mec; ··········, calculated using DMEH-mec changing k_7 value to $k_7 = 8.0 \times 10^{12}$ exp (- 12.5 kcal/RT) cm^{3}mol^{-1}s^{-1} [20].

Fig. 1b. Sensitivity spectra (pS) [30] for DME, C_2H_6, C_2H_4, C_2H_2, CH_4, and H_2 concentrations at 1300 K at 1000 μs using mixture A7. The solid bars show the result of multiplying the indicated rate constants by 0.2, while the open bars show the result of multiplying the indicated rate constants by 5. The horizontal axis shows the reaction numbers.

3.3. Time-resolved IR-emission at 4.24 μm

IR-emission profiles at 4.24 μm were measured for mixtures A6, A8 - A11, and A12. Typical IR emission profiles at 4.24 μm for fuel-rich mixture A6, stoichiometric mixture A8, and fuel-lean mixtures A9, A10, and A12 are shown in Figs. 6a, 7, 8, 9a, and 10, where E_{200}, E_{500}, E_{900}, E_{1000}, and E_t are the emission intensity at 200 μs, 500 μs, 900 μs, 1000 μs, and t μs, respectively. The CO_2 profiles exhibit a rapid increase after a period following shock-heating, as shown in Figs. 6a, 7 - 9a, and 10. An induction time τ_{CO2} was defined as the elapsed time between the reflected shock arrival and the onset of the rapid infrared emission increase, determined from the intersection of the tangent to the curve at its inflection point with the pre-shock base line. Plots of log τ_{CO2} vs. 1/T obtained with mixtures A6, A8 - A11, and A12 are shown in Fig. 11.

3.4. Time-resolved OH absorption at 306.7 nm
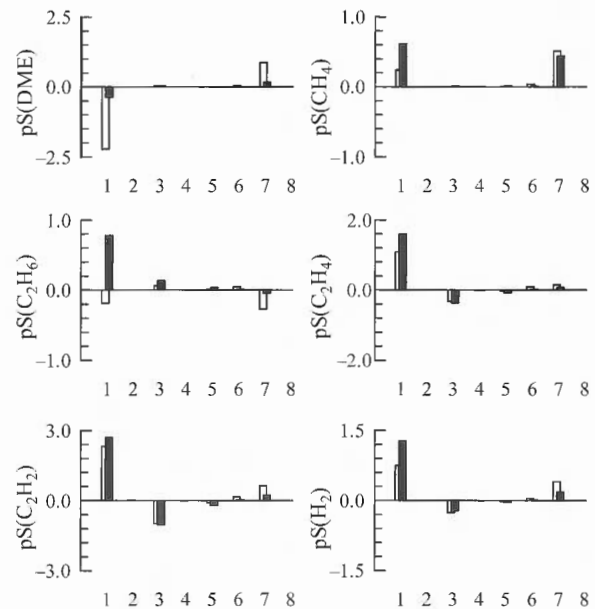
The OH absorption profiles at 306.7 nm were measured

with mixture A13. A typical profile in DME oxidation is shown in Fig. 12a. The OH absorption profile exhibits a rapid increase after a period following shock heating. An induction time τ_{OH} was defined as the elapsed time between reflected shock arrival and the onset of the rapid absorption increase, determined from the intersection of the tangent to the curve at its inflection point with the pre-shock base line. The induction period τ_{OH} observed with mixture A13 is shown in Fig. 13, together with the results of oxidation of mixture 1 % H_2, 1 % O_2 diluted with Ar. It was found that the OH formation was inhibited by adding DME under our experimental conditions below about 1500 K, as shown in Fig. 13.

3.5. Time-resolved UV absorption at 216 nm

To examine CH_3 radical production, the UV absorption profiles at 216 nm were measured using mixture A8. We could determine precisely the rate of CH_3 production and consumption using mixture A8 because this mixture gave the highest CH_3 concentration. A typical absorption profile is shown in Fig. 14. The experimental errors of the profiles are less than ± 2 %. In order to determine the absorption by reactant and each stable product at 216 nm, the extinction coefficients were measured using mixtures, 4 % DME, 1 % CH_2O, 0.4 % 1,3-C_4H_6, 4 % C_2H_4, 4 % C_2H_2, 5 % CO, and 5 % CO_2, respectively, diluted with Ar. The extinction
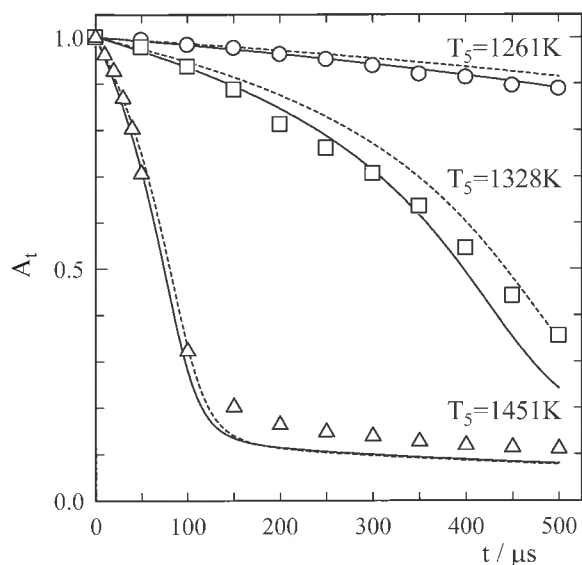
Fig. 2a. Comparison of the observed laser-absorption curves with those calculated at low, middle and high temperatures using mixture A5. $\bigcirc$, 1261 K, 1.98 atm, 1.91×10^{-5} mol/cm^3; $\square$, 1328 K, 2.17 atm, 1.99×10^{-5} mol/cm^3; $\triangle$, 1451 K, 2.54 atm, 2.13×10^{-5} mol/cm^3; ———, calculated using MEH-mec; ············, calculated using DMEH-mec changing k_7 value to $k_7 = 8.0 \times 10^{12}$ exp (- 12.5 kcal/RT) cm^{3}mol^{-1}s^{-1} [20].
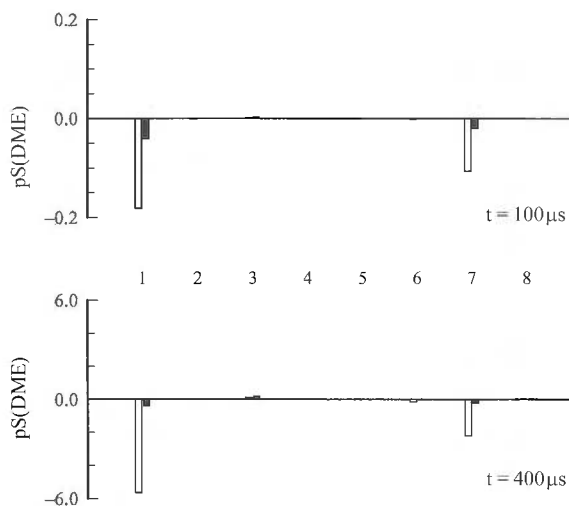
Fig. 2b. Sensitivity spectra (pS) [30] for DME concentration at 1328 K at 100 and 400 μs using mixture A5. The solid bars show the result of multiplying the indicated rate constants by 0.2, while the open bars show the result of multiplying the indicated rate constants by 5. The horizontal axis shows the reaction numbers.
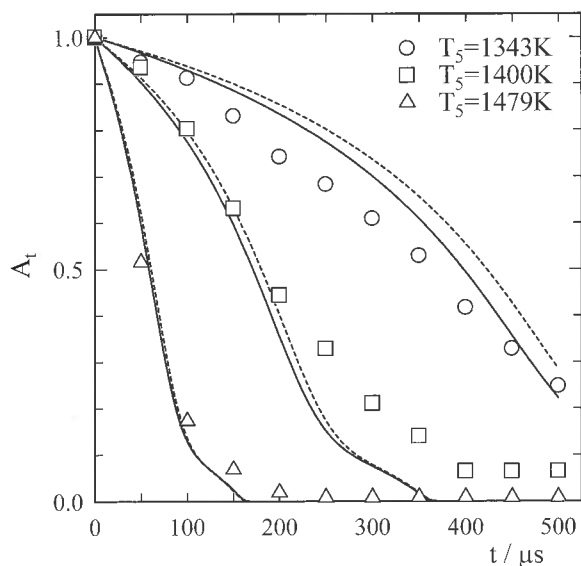

Fig. 3a. Comparison of the observed laser-absorption curves with those calculated at low, middle and high temperatures using mixture A6. $\bigcirc$, 1343 K, 1.91 atm, 1.73×10^{-5} mol/cm^3; $\square$, 1400 K, 2.05 atm, 1.78×10^{-5} mol/cm^3; $\triangle$, 1479 K, 2.24 atm, 1.85×10^{-5} mol/cm^3; ———, calculated using DMEH-mec; ············, calculated using ch DMEH-mec changing k_7 value to $k_7 = 8.0 \times 10^{12}$ exp (- 12.5 kcal/RT) cm^{3}mol^{-1}s^{-1} [20].
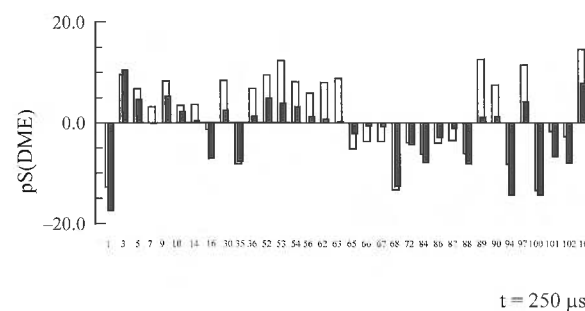

Fig. 3b. Sensitivity spectra (pS) [30] for DME concentration at 1440 K at 250 μs using mixture A6. The solid bars show the result of multiplying the indicated rate constants by 0.2, while the open bars show the result of multiplying the indicated rate constants by 5. The horizontal axis shows the reaction numbers.

coefficients were calculated from the absorption at the reflected shock front. The equations obtained were log I_a (1,3-C$_4$H$_6$) = - 1.97×10^{-4}T + 7.26 cm^{2}mol^{-1}, log I_a (C$_2$H$_4$) = 1.67×10^{-3}T + 2.10 cm^{2}mol^{-1}, log I_a (CO$_2$) = 7.70×10^{-4}T +

2.68 cm^{2}mol^{-1}, and log I_a (C$_2$H$_2$) = 7.40×10^{-4}T + 3.70 cm^{2}mol^{-1} for 1,3-C$_4$H$_6$, C$_2$H$_4$, CO$_2$, and C$_2$H$_2$, respectively. Absorption by DME, CH$_2$O, CO$_2$ and CO was too small to detect. The equation log I_a (CH$_3$) = 6.26 cm^{2}mol^{-1} [20] was used for the CH$_3$ radical. These equations were used in the simulations. From the above equations, the absorption of CH$_3$ at 216 nm was found to be much greater than that of stable products. Consequently, we could determine the kinetic behavior of the CH$_3$ radical from the absorption profiles at 216 nm.
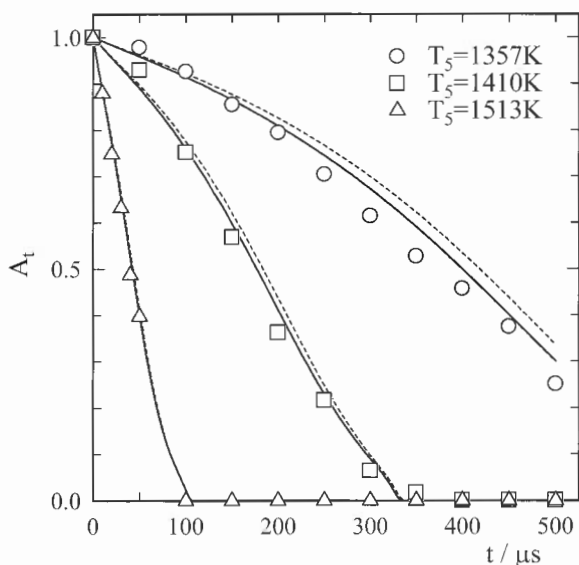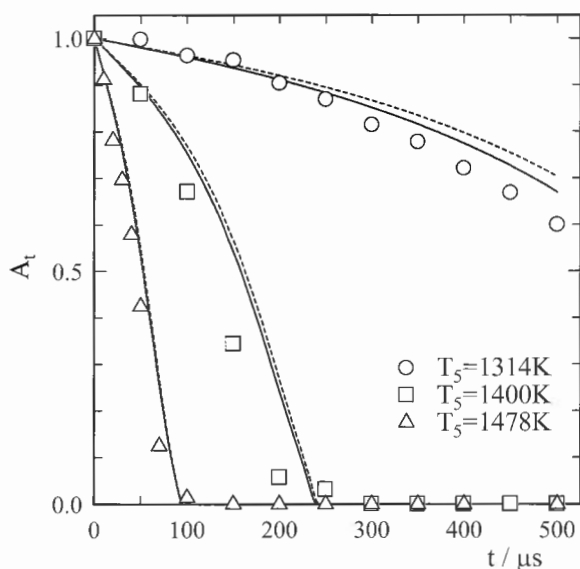
Fig. 4a. Comparison of the observed laser-absorption curves with those calculated at low, middle and high temperatures using mixture A8. ○, 1357 K, 1.78 atm, 1.60 x 10^{-5} mol/cm^3; □, 1410 K, 1.90 atm, 1.64 x 10^{-5} mol/cm^3; △, 1513 K, 2.13 atm, 1.71 x 10^{-5} mol/cm^3; ——, calculated using DMEH-mec; ··········, calculated using DMEH-mec changing k_7 value to $k_7 = 8.0$ x 10^{12} exp (- 12.5 kcal/RT) cm^{3}mol^{-1}s^{-1} [20].

Fig. 4b. Sensitivity spectra (pS) [30] for DME concentration at 1410 K at 100 and 200 μs using mixture A8. The solid bars show the result of multiplying the indicated rate constants by 0.2, while the open bars show the result of multiplying the indicated rate constants by 5. The horizontal axis shows the reaction numbers.

Fig. 5. Comparison of the observed laser-absorption curves with those calculated at low, middle and high temperatures using mixture A9. ○, 1314 K, 1.74 atm, 1.62 x 10^{-5} mol/cm^3; □, 1400 K, 1.94 atm, 1.69 x 10^{-5} mol/cm^3; △, 1478 K, 2.12 atm, 1.75 x 10^{-5} mol/cm^3; ——, calculated using DMEH-mec; ··········, calculated using DMEH-mec changing k_7 value to $k_7 = 8.0$ x 10^{12} exp (- 12.5 kcal/RT) cm^{3}mol^{-1}s^{-1} [20].

3.6. Reaction Mechanism

A new DME oxidation mechanism was compiled by combining a DME pyrolysis mechanism [20] with an oxidation mechanism including oxidation of C_1- and C_2-
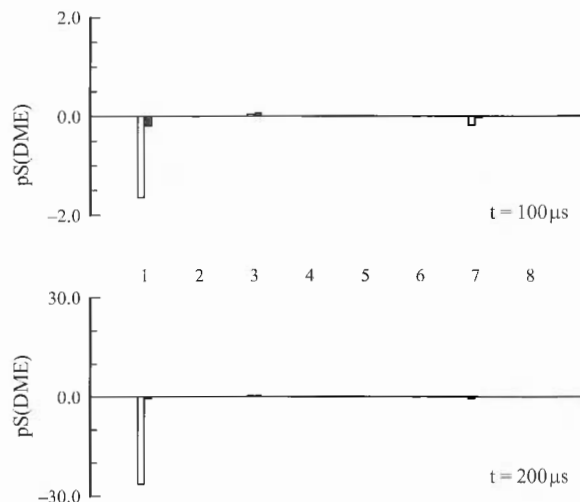
hydrocarbons, CH_2O, and CH_2CO reported elsewhere [9-13,21,22]. By using this mechanism and new information for the DME pyrolysis and oxidation [1-4], we identified a mechanism and rate constant expressions that could predict, (1) the pyrolysis results obtained over a wide concentration range, from 0.1 % DME to 4 % DME, (2) oxidation results obtained under very fuel-rich (mixture A5), stoichiometric (mixture A8), and very fuel-lean (mixtures A10 and A12) conditions, and (3) results obtained using H_2-O_2 mixtures containing DME (mixture A13). The final mechanism and rate constant expressions with 178 reaction steps and 53 species (DMEH-mec) were determined. They are provided at the World Wide-Web address: http://chem.sci.ehime-u.ac.jp/%7Ephychem1/hidaka/home.htm. The simulation results using the final mechanism reproduced all our data within experimental error, as shown in Figs. 1a-15 and 16.

4. Discussion

4.1. k_1 Value

The reported rate constant expression $k_1 = 5.20$ x 10^{14} exp (- 75.0 kcal/RT) s^{-1} [20] evaluated from the best fit to the DME pyrolysis findings was applied for our experimental findings in the DME oxidation. This k_1 expression was able to explain well our oxidation findings within experimental error. The profiles for the 0.2 % DME mixture diluted with Ar (Fig. 16) were sensitive to the variation in the rate constant of reaction 1, as shown in Fig. 1 of Ref. 20. The consumption
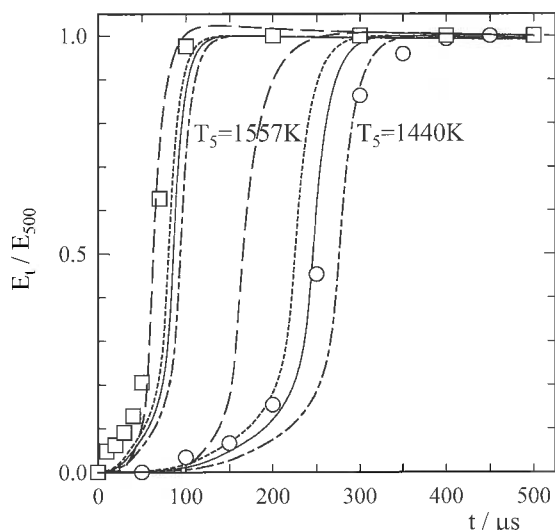
Fig. 6a. Comparison of the time-profiles measured at 4.24 μm with those calculated using mixture A6. $\bigcirc$, observed at 1440 K and 2.14 atm and total density, 1.81×10^{-5} mol/cm³; $\square$, observed at 1557 K and 2.44 atm and total density, 1.91×10^{-5} mol/cm³; ———, calculated using DMEH-mec; ··········, calculated using DMEH-mec changing k_1 value to the maximum value, $k_1 = 6.5 \times 10^{14}$ exp (- 75.0 kcal/RT) s⁻¹ [20]; —·—·—, calculated using DMEH-mec changing k_1 value to the minimum value, $k_1 = 3.9 \times 10^{14}$ exp (-75.0 kcal/RT) s⁻¹ [20]; — — —, calculated using Fischer et al. mechanism [4].
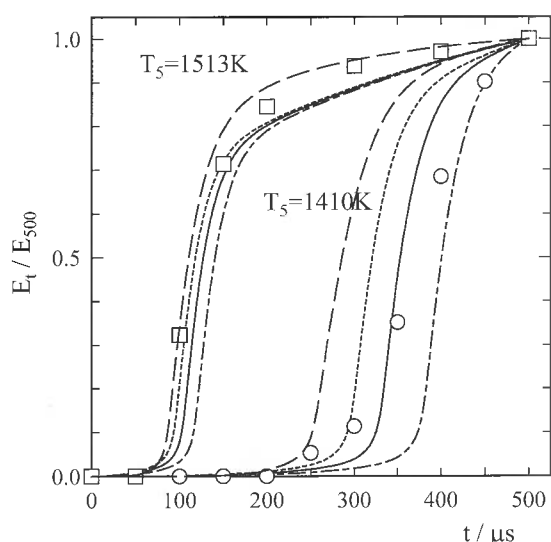

Fig. 7. Comparison of the time-profiles measured at 4.24 μm with those calculated using mixture A8. $\bigcirc$, observed at 1410 K and 1.90 atm and total density, 1.64×10^{-5} mol/cm³; $\square$, observed at 1513 K and 2.13 atm and total density, 1.71×10^{-5} mol/cm³; ———, calculated using DMEH-mec; ··········, calculated using DMEH-mec changing k_1 value to the maximum value, $k_1 = 6.5 \times 10^{14}$ exp (- 75.0 kcal/RT) s⁻¹ [20]; —·—·—, calculated using DMEH-mec changing k_1 value to the minimum value, $k_1 = 3.9 \times 10^{14}$ exp (- 75.0 kcal/RT) s⁻¹ [20]; — — —, calculated using Fischer et al. mechanism [4].
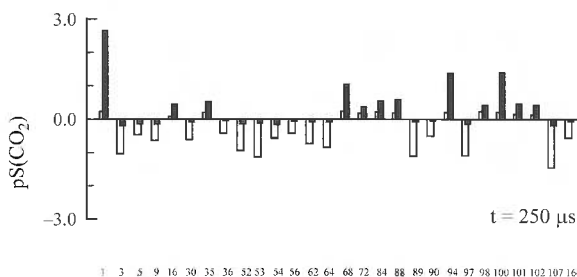

Fig. 6b. Sensitivity spectra (pS) [30] for CO_2 concentration at 1440 K at 250 μs using mixture A6. The solid bars show the result of multiplying the indicated rate constants by 0.2, while the open bars show the result of multiplying the indicated rate constants by 5. The horizontal axis shows the reaction numbers.

of DME and the production of carbon monoxide were also very sensitive to the rate constant of reaction 1, as shown in Fig. 6b of Ref. 20. All the profiles for the oxidation mixtures are also sensitive to the variation in the rate constant of reaction 1, as shown in Figs. 1b - 4b, 6b, 8b, 9b, and 12b. The profiles for mixtures A6 (2 % DME, 3 % O_2 95.0 % Ar) and A8 (1 % DME, 3 % O_2 96 % Ar) are also sensitive to the variation in the rate constant of reaction 1, as shown in Figs. 4b and 6b. To explain all our experimental pyrolysis and oxidation data consistently, reaction 1 with $k_1 = 5.2 \times 10^{14}$ exp (- 75.0 kcal/RT) s⁻¹ is indispensable. The maximum value, $k_1 = 6.5 \times 10^{14}$ exp (- 75.0 kcal/RT) s⁻¹, and minimum value, $k_1 = 3.9 \times 10^{14}$ exp (- 75.0 kcal/RT) s⁻¹, were determined. This value is consistent with that of Fischer et al. recently reported [4]. Reaction 1 is fall-off region under our experimental conditions.

4.2. k_2 Value

Reaction 2 with $k_2 = 4.1 \times 10^{13}$ exp (- 44.9 kcal/RT) cm³mol⁻¹s⁻¹ [3] was reported as a reaction between DME and O_2.

$$CH_3OCH_3 + O_2 \rightarrow CH_3OCH_2 + HO_2 \qquad (2)$$
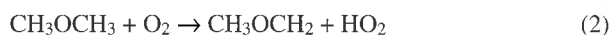
When the reported value $k_2 = 4.1 \times 10^{13}$ exp (- 44.9 kcal/RT) cm³mol⁻¹s⁻¹ [3] are used, little influence on species concentration in the simulations is confirmed ever for mixture A10. So, we are not able to examine this value from our experimental results. This reaction is not important under our experimental conditions.

4.3. k_3 Value

When a small amount of DME is added to H_2-O_2 mixture, reaction 100, $O_2 + H \rightarrow OH + O$ and reaction 3 are competitive.
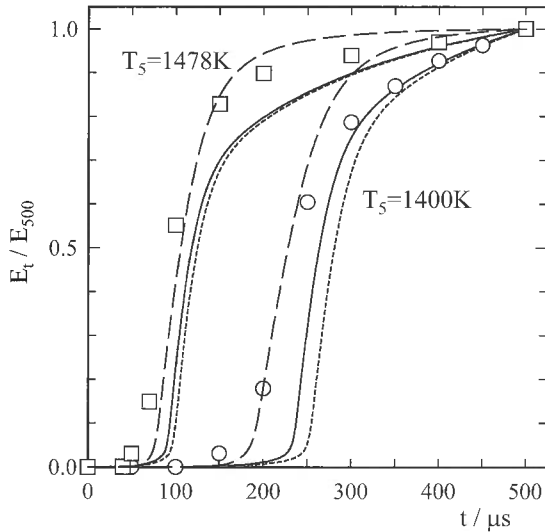
Fig. 8a. Comparison of the CO_2 profiles measured at 4.24 μm with those calculated using mixture A9. ◯, observed at 1400 K, 1.94 atm and total density, 1.69 x 10^{-5} mol/cm³; □, observed at 1478 K, 2.12 atm and total density, 1.75 x 10^{-5} mol/cm³; ———, calculated using DMEH-mec; ············, calculated using DMEH-mec changing the k_3 value to k_3 = 4.8 x $10^7T^{1.9}$ exp (- 3.7 kcal/RT) cm³mol⁻¹s⁻¹; — — —, calculated using Fischer et al. mechanism [4].
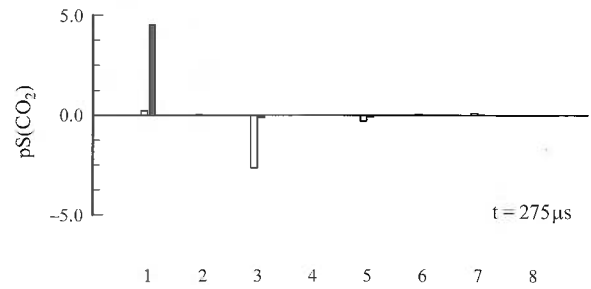

Fig. 8b. Sensitivity spectra (pS) [30] for DME concentration at 1478 K at 275 μs using mixture A9. The solid bars show the result of multiplying the indicated rate constants by 0.2, while the open bars show the result of multiplying the indicated rate constants by 5. The horizontal axis shows the reaction numbers.
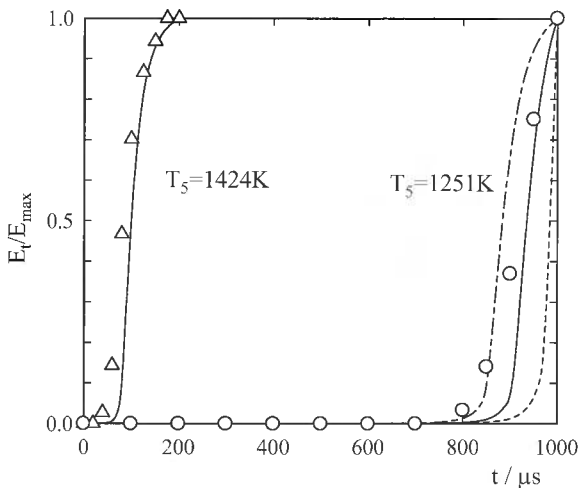
Fig. 9a. Comparison of the CO_2 profiles measured at 4.24 μm with those calculated using mixture A10. ◯, observed at 1251 K, 2.05 atm and total density, 1.99 x 10^{-5} mol/cm³; △, observed at 1424 K, 2.57 atm and total density, 2.20 x 10^{-5} mol/cm³; ———, calculated using DMEH-mec; — — —, calculated using DMEH-mec changing the k_3 value to reported maximum value k_3 = 4.8 x $10^7T^{1.9}$ exp (-3.7 kcal/RT) cm³mol⁻¹s⁻¹ [20]; —·—·—, calculated using DMEH-mec changing the k_5 value to k_5 = 9.35 x $10^5T^{2.29}$ exp (0.78 kcal/RT) cm³mol⁻¹s⁻¹ [4].

Fig. 9b. Sensitivity spectra (pS) [30] for CO_2 concentration at 1251 K at 900 μs using mixture A10. The solid bars show the result of multiplying the indicated rate constants by 0.2, while the open bars show the result of multiplying the indicated rate constants by 5. The horizontal axis shows the reaction numbers.
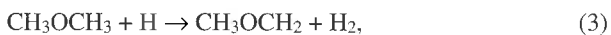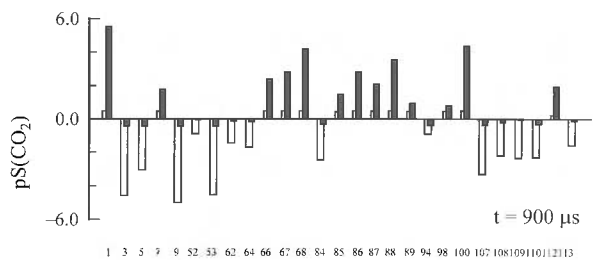
$$CH_3OCH_3 + H \rightarrow CH_3OCH_2 + H_2, \qquad (3)$$

The calculated profiles for mixtures 1 % H_2, 1 % O_2, 0.1 % DME, 97.9 % Ar are very sensitive to the k_3 value, as shown in Fig. 12b. The reliability of the rate constant k_{100} = 9.75 x

10^{13} exp (- 14.9 kcal/RT) cm³mol⁻¹s⁻¹ used for reaction 100 is high, and this value can reproduce the observed τ_{OH} in the H_2 oxidation, as shown in Fig. 13. Analyzing the data obtained using H_2-O_2-DME mixture, we are able to obtain a useful information for the rate constant of reaction between the DME and H atom. The τ_{OH} simulated using our previous reported value k_3 = 3.2 x $10^7T^{1.9}$ exp (- 3.7 kcal/RT) cm³mol⁻¹s⁻¹ [20] are also the best fits to our data, as shown in Figs. 12a and 13. The calculated profiles for mixtures A9 and A10 are also very sensitive to the k_3 value, as shown in Figs. 8b and 9b. The CO_2 and the At profile for mixture A9 simulated using k_3 = 3.2 x $10^7T^{1.9}$ exp (- 3.7 kcal/RT) cm³mol⁻¹s⁻¹ are also the best fits to our observed data, as shown in Figs. 5 and 8a.
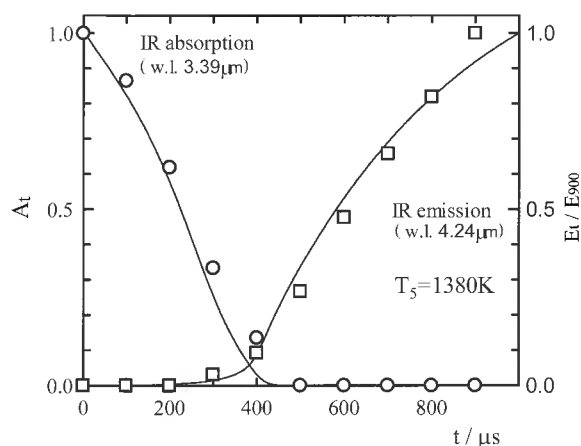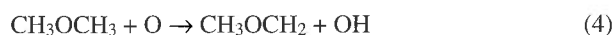
Fig. 10. Comparison of both the laser-absorption profile at 3.39 μm and the CO_2 profile at 4.24 μm observed at 1380 K and 1.76 atm (total density, 1.56 x 10^{-5} mol/cm^3) with those calculated for mixture A12. The solid line represents model calculations using DMEH-mec.

Fig. 11. Comparison of induction times observed at 4.24 μm with those calculated for mixtures A6, A8 - A11, and A12. The total pressure and density ranges used are 1.50 - 2.66 atm and 1.46 x 10^{-5} - 2.23 x 10^{-5} mol/cm^3, respectively. $\bigcirc$, observed using mixture A8; $\triangle$, observed using mixture A6; $\square$, observed using mixture A9; $\bullet$, observed using mixture A11; $\blacklozenge$, observed using mixture A12; $\diamondsuit$, observed using mixture A10; ———, calculated using DMEH-mec.

Furthermore, the CO_2 profile for mixture A10 simulated using $k_3 = 3.2$ x $10^7T^{1.9}$ exp (- 3.7 kcal/RT) cm^{3}mol^{-1}s^{-1} is the best fit to our observed data, as shown in Fig. 9a. This evaluated value was also able to predict DME pyrolysis data within experimental error, as shown in Ref. 20. This value is in good agreement with the value of Fischer et al [4] but is somewhat lower than value of Curran et al. [3]. The extrapolated value of $k_3 = 3.2$ x $10^7T^{1.9}$ exp (- 3.7 kcal/RT) cm^{3}mol^{-1}s^{-1} was in good agreement with the values of Faubel et al. [23] and Lee et al. [24] at low temperatures, as shown in Fig. 15 of Ref. 20.

4.4. k_4 Value

Reaction 4 played a role in the DME consumption in the oxidation at high temperatures: this reaction may consume about 3 % of the DME concentration at 1412 K and 200 μs using mixture A7. However, none of our observed data are sensitive to the above k_4 values, as shown in Figs. 1b, 2b, 3b, 4b, 6b, 8b, 9b, and 12b. So, we are not able to examine this value from our experimental results.

$$CH_3OCH_3 + O \rightarrow CH_3OCH_2 + OH \qquad (4)$$

Curran et al. [3] reported $k_4 = 1.86$ x $10^{-3}T^{5.3}$ exp (0.11 kcal/RT) cm^{3}mol^{-1}s^{-1}. Recently, Fischer et al [4] also used this expression for the detailed chemical model of the DME oxidation over the wide range of conditions. However, the k_4 value is 1.2 x 10^{14} cm^{3}mol^{-1}s^{-1} at 1500 K. This value is considered to be too large because the rate constant value for the reaction of atomic oxygen with DME will be similar to that for the reaction of atomic hydrogen with DME: the rate constant value for the reaction of atomic oxygen with CH$_4$ or
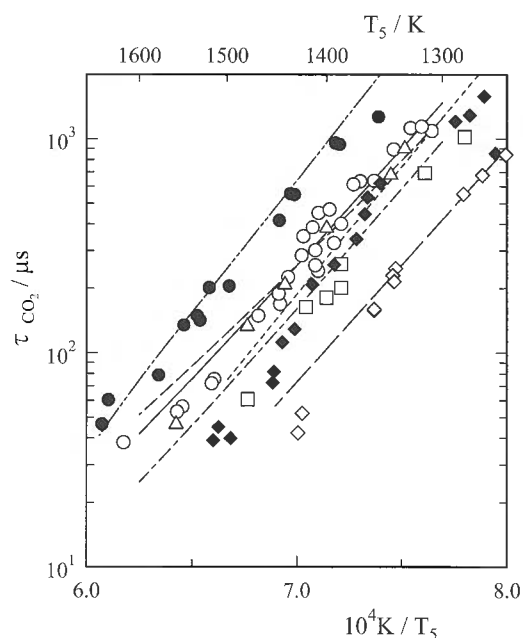
C_2H_6 is similar to that for the reaction of atomic hydrogen with CH$_4$ or C_2H_6 [21,22]. Hence, we assumed a tenth value of Curran et al. [3] for the rate constant k_4. This rate constant is also able to reproduce our experimental results. Even if the Curran et al. value [3] was used for our simulations, our experimental results were reproduced.

4.5. k_5 Value

Reaction 5 has been reported as a reaction between OH radicals and DME.

$$CH_3OCH_3 + OH \rightarrow CH_3OCH_2 + H_2O \qquad (5)$$

This reaction plays an important role in DME consumption in the oxidation at high temperatures: this reaction may consume about 16 % of the DME concentration at 1412 K and 200 μs using mixture A7. Our data observed at 1251 K using mixture A10 is very sensitive to the k_5 value, as shown in Fig. 9b. Our data observed at 1348 K using mixture A13 is also very sensitive to the k_5 value, as shown in Fig. 12b. The best fits to our observed data were obtained by using $k_5 = 4.5$ x 10^{14} exp (- 6.1 kcal/RT) cm^{3}mol^{-1}s^{-1}. Our data in Fig. 12a is also very sensitive to the k_1, k_3, and k_{100} values, as shown in Fig. 12b. These maximum values and minimum values [20]
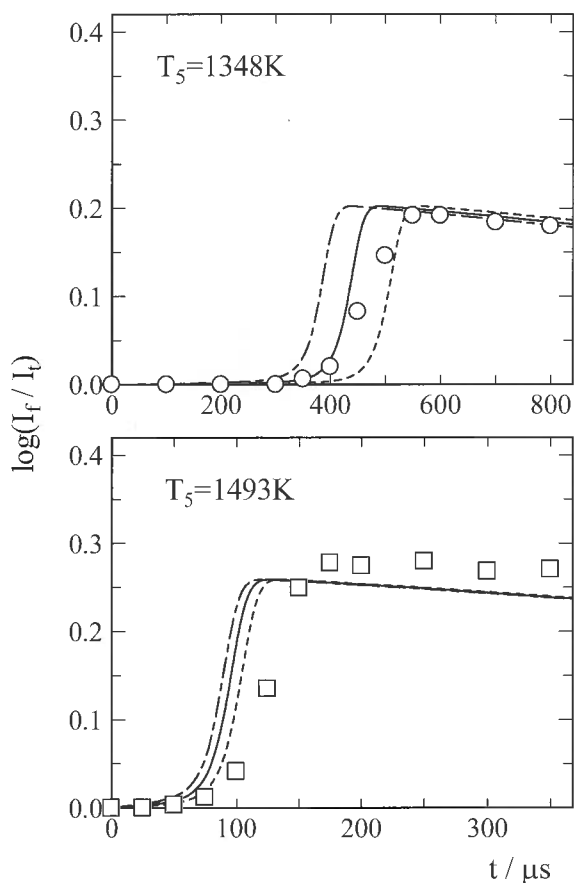
Fig. 12a. Comparison of the time-profiles measured at 306.7 nm with those calculated using mixture A13. ○, observed at 1348 K, 1.60 atm and total density, 1.45×10^{-5} mol/cm^3; □, observed at 1493 K, 1.89 atm and total density, 1.54×10^{-5} mol/cm^3; ———, calculated using DMEH-mec; − − −, calculated using DMEH-mec changing the k_3 value to reported maximum value $k_3 = 4.8 \times 10^7 T^{1.9}$ exp (- 3.7 kcal/RT) cm^3 mol^{-1}s^{-1} [20]; −·−·−, calculated using DMEH-mec changing the k_5 value to $k_5 = 9.35 \times 10^5 T^{2.29}$ exp(0.78 kcal/RT) cm^{3}mol^{-1}s^{-1} [4].

for reactions 1 and 3 and the value reported for reaction 100 [4,19] were used to estimate an uncertainty for k_5. The uncertainty of ± 30 % was estimated for k_5. The uncertainty coming from an analytical error and an error in calculated shock temperatures is ± 20 %. The evaluated k_5 has an uncertainty of ± 50 %. This value is about 2.5 times that of Fischer et al [4]. If we assumed Fischer et al. value [4] for k_5, simulated profiles are faster than the observed ones, as shown in Figs. 9(a) and 12(a). So, we adopted the value 4.5×10^{14} exp (- 6.1 kcal/RT) cm^{3}mol^{-1}s^{-1} for the k_5.

4.6. k_6 Value

It has been reported that abstraction of HO$_2$ radicals is quite important in the oxidation process in a jet-stirred reactor over the temperature range of 800 K - 1300 K at 1 and 10 atm [3].
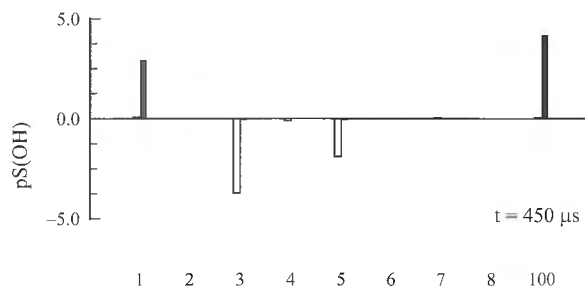

Fig. 12b. Sensitivity spectra (pS) [30] for OH radical concentration at 1348 K at 450 μs using mixture A13. The solid bars show the result of multiplying the indicated rate constants by 0.2, while the open bars show the result of multiplying the indicated rate constants by 5. The horizontal axis shows the reaction numbers.

$$CH_3OCH_3 + HO_2 \rightarrow CH_3OCH_2 + H_2O_2 \qquad (6)$$

A possibility of reaction 6 under our experimental conditions was examined using reaction 6 with $k_6 = 1.00 \times 10^{13}$ exp (- 17.7 kcal/RT) cm^{3}mol^{-1}s^{-1} [3]. None of our observed data are sensitive to the above k_6 value. The DME consumption by reaction 6 in the oxidation at high temperatures is little: maximum consumption of DME by reaction 6 is about 1 % concentration at 1251 K and 700 μs using mixture A10. Even if the value of $k_6 \times 5$ was assumed, the simulated profiles or species concentrations did not change. So, we are not able to examine this value from our experimental results. Reaction 6 is considered to be unimportant under our experimental conditions.

4.7. k_7 Value

$$CH_3OCH_3 + CH_3 \rightarrow CH_3OCH_2 + CH_4 \qquad (7)$$

The A_t profiles for mixture A5 (Fig. 2a) mainly come from the DME consumption and are also sensitive to the variation in the rate constant of reaction 7, as shown in Fig. 2b. The concentration distribution of CH$_4$ and C$_2$H$_6$ is also sensitive to the k_7 value, as shown in Fig. 1b. The best-fit value of reaction 7 to these observed results is $k_7 = 1.0 \times 10^3 T^{3.0}$ exp (- 8.4 kcal/RT) cm^{3}mol^{-1}s^{-1}. The value $k_7 = 1.0 \times 10^3 T^{3.0}$ exp (- 8.4 kcal/RT) cm^{3}mol^{-1}s^{-1} reproduces more closely those observed, as shown in Figs. 2a, 3a, and 4a. However, the use of this k_7 value gives a little large volume of methane as compared with that observed, as shown in Fig. 1a, and give smaller A_t values than those observed, as shown in Fig. 15. On the other hand, the reported value, $k_7 = 8.0 \times 10^{12}$ exp (- 12.5 kcal/RT) cm^{3}mol^{-1}s^{-1} [20], reproduced those observed, as shown in Figs. 1 and 15. However, the A_t calculated using the reported value, $k_7 = 8.0 \times 10^{12}$ exp (- 12.5 kcal/RT)
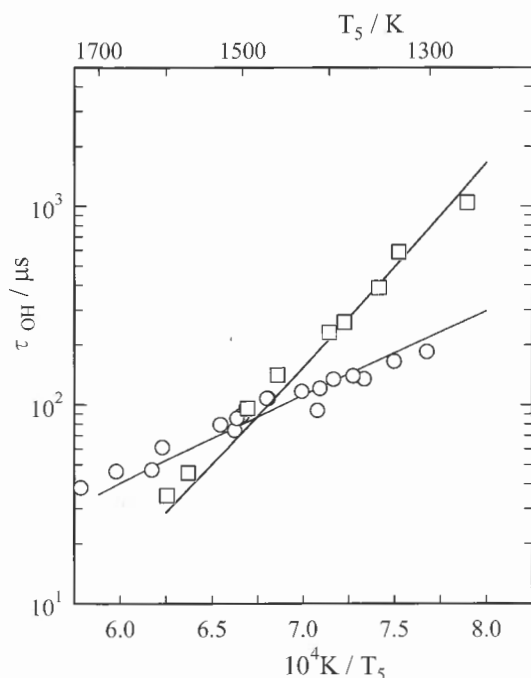
Fig. 13. Comparison of induction times observed using mixtures, (1.0 % H_2, 1.0 % O_2, 98.0 % Ar; $\bigcirc$) and (1.0 % H_2, 1.0 % O_2, 0.1 % DME, 97.9 % Ar; $\square$) at 306.7 nm with those calculated. The total pressure and density ranges used are 1.42 - 2.10 atm and 1.38 x 10^{-5} - 1.60 x 10^{-5} mol/cm^3, respectively. ———, calculated using DMEH-mec.
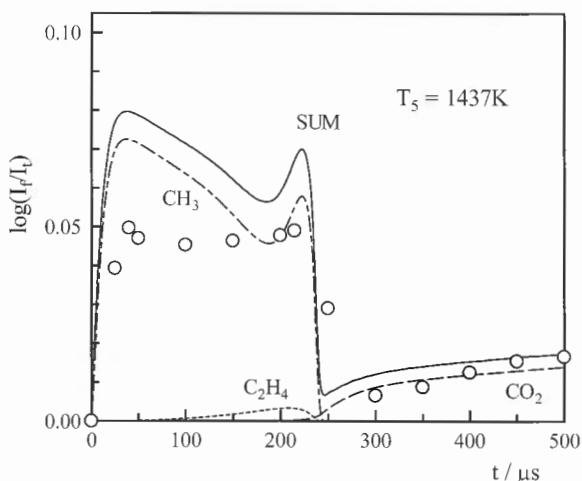

Fig. 14. Comparison of the UV-absorption curves observed at 216 nm with those calculated at 1437 K, 1.96 atm, and 1.66 x 10^{-5} mol/cm^3, using mixture A8. $\bigcirc$, observed; ———, sum calculated using DMEH-mec; —·—·—, absorption due to CH_3; ············, absorption due to C_2H_4; — — —, absorption due to CO_2.

Fig. 15. Comparison of the observed laser-absorption curves (symbol) with those calculated at low, middle and high temperatures using mixture A1. $\square$, 1305 K, 2.06 atm, 1.92 x 10^{-5} mol/cm^3; $\triangle$, 1413 K, 2.38 atm, 2.05 x 10^{-5} mol/cm^3; $\bigcirc$, 1501 K, 2.64 atm, 2.14 x 10^{-5} mol/cm^3; ———, calculated using DMEH-mec; ············, calculated using DMEH-mec changing k_7 to k_7 = 8.0 x 10^{12} exp (- 12.5 kcal/RT) cm^{3}mol^{-1}s^{-1} [20].

cm^{3}mol^{-1}s^{-1} [20], are a little larger than those observed, as shown in Figs. 2a, 3a, and 4a. On the whole, the best-fit value of reaction 7 to both the observed pyrolysis and oxidation data is k_7 = 1.0 x $10^3T^{3.0}$ exp (- 8.4 kcal/RT) cm^{3}mol^{-1}s^{-1}, which is the maximum value for the reported rate constant k_7 [20]. So, we adopted the value 1.0 x $10^3T^{3.0}$ exp (- 8.4 kcal/RT) cm^{3}mol^{-1}s^{-1} for the k_7. The extrapolated value of k_7 = 1.0 x $10^3T^{3.0}$ exp (- 8.4 kcal/RT) cm^{3}mol^{-1}s^{-1} at low temperatures is in good agreement with the values of Marcus et al. [25], Trotman-Dickenson and Steacie [26], and Loucks [27], Pacey et al. [28], and Held et al. [29]. Our value at 1100 K is also in good agreement with the values of Curran et al. [3] or Fischer et al [4]. However, our value at 1500 K is about half those of Curran et al. [3] and Fischer et al [4].

4.8. Reactions 181 - 185

Reactions 181 - 185 of CH_3OCH_2 radical with O_2, HO_2, CH_2O, CH_3O and CH_3CHO have been reported [3,4].

$$CH_3OCH_2 + CH_3O \rightarrow CH_3OCH_3 + CH_2O \quad (181)$$

$$CH_3OCH_2 + CH_2O \rightarrow CH_3OCH_3 + CHO \quad (182)$$

$$CH_3OCH_2 + CH_3CHO \rightarrow CH_3OCH_3 + CH_3CO \quad (183)$$

$$CH_3OCH_2 + HO_2 \rightarrow CH_3OCH_2O + OH \quad (184)$$

$$CH_3OCH_2 + O_2 \rightarrow CH_3OCH_2O_2 \quad (185)$$

Even if the reported values, k_{181} = 2.4 x 10^{13} cm^{3}mol^{-1}s^{-1} [4], k_{182} = 5.5 x $10^3T^{2.8}$ exp (- 5.9 kcal/RT) cm^{3}mol^{-1}s^{-1} [4], k_{183} = 1.3 x 10^{12} exp (- 8.5 kcal/RT) cm^{3}mol^{-1}s^{-1} [4], k_{184} = 9.0 x 10^{12} cm^{3}mol^{-1}s^{-1} [4], and k_{185} = 2.0 x 10^{12} cm^{3}mol^{-1}s^{-1} [4], were assumed, no influence on species concentration in the simulations was confirmed under our experimental
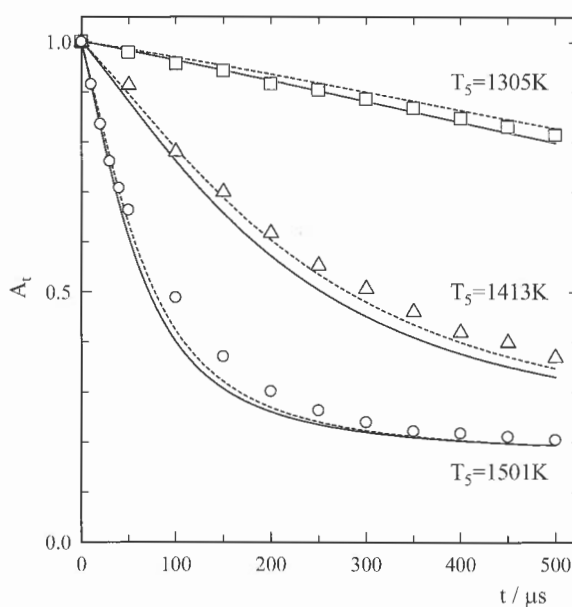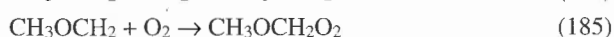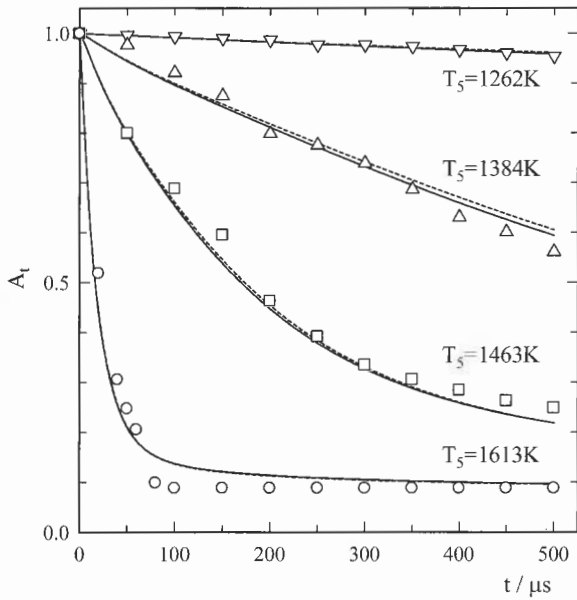
Fig. 16. Comparison of the observed laser-absorption curves (symbol) with those calculated at low, middle and high temperatures using mixture A4. ∇, 1262 K, 1.42 atm, 1.38×10^{-5} mol/cm^3; $\triangle$, 1384 K, 1.65 atm, 1.46×10^{-5} mol/cm^3; $\square$, 1463 K, 1.81 atm, 1.51×10^{-5} mol/cm^3; $\bigcirc$, 1613 K, 2.10 atm, 1.59×10^{-5} mol/cm^3; ———, calculated using DMEH-mec; ··········, calculated using DMEH-mec changing k_7 to $k_7 = 8.0 \times 10^{12}$ exp (- 12.5 kcal/RT) cm^{3}mol^{-1}s^{-1} [20].

Fig. 17. Flow diagram for DME oxidation in stoichiometric DME-O$_2$-Ar mixture at T_5 = 1300 K, P_5 = 1.66 atm.

conditions. These reactions were not important in explaining data under our experimental conditions.

4.9. Reactions 9 - 178

The rate constants of reactions 9-178 used in DMEH-mec are the same as those used for modeling C$_2$H$_6$, C$_2$H$_2$, and CH$_2$O oxidation [8,10,22]. The rate constants of reactions 9-178 used are the same as those used in the most recent pyrolysis and oxidation sub-mechanisms for formaldehyde [10], methane [21], ethane [22], ethylene [11], and acetylene [8], which were the main stable intermediate species in the DME oxidation. Under our experimental conditions, these reactions played a role in the DME oxidation. The CO$_2$ formation in mixture A10 (very fuel-lean condition) is very sensitive to the rate constants of reactions 1, 3, 5, 7, 9, 52, 53, 62, 64, 66, 67, 68, 84-89, 94, 98, 100, 107, 108, 109, 110, 112, and 113, as shown in Fig. 9b.

CH$_3$ + CH$_3$ (+ M) $\rightarrow$ C$_2$H$_6$ (+ M)	(9)
H + CH$_3$ (+ M) $\rightarrow$ CH$_4$ (+ M)	(52)
CH$_4$ + O$_2$ $\rightarrow$ CH$_3$ + HO$_2$	(53)
CH$_3$ + O $\rightarrow$ CH$_2$O + H	(62)
CH$_3$ + OH $\rightarrow$ CH$_2$O + H$_2$	(64)
CH$_3$ + O$_2$ $\rightarrow$ CH$_3$O + O	(66)
CH$_3$ + O$_2$ $\rightarrow$ CH$_2$O + OH	(67)
CH$_3$ + HO$_2$ $\rightarrow$ CH$_3$O + OH	(68)
CH$_2$O + H $\rightarrow$ CHO + H$_2$	(84)
CH$_2$O + O $\rightarrow$ CHO + OH	(85)
CH$_2$O + OH $\rightarrow$ CHO + H$_2$O	(86)
CH$_2$O + HO$_2$ $\rightarrow$ CHO + H$_2$O$_2$	(87)
CH$_2$O + CH$_3$ $\rightarrow$ CHO + CH$_4$	(88)
CHO + M $\rightarrow$ CO + H + M	(89)
CHO + O$_2$ $\rightarrow$ HO$_2$ + CO	(94)
CO + OH $\rightarrow$ CO$_2$ + H	(98)
O$_2$ + H $\rightarrow$ OH + O	(100)
HO$_2$ + H $\rightarrow$ H$_2$ + O$_2$	(107)
HO$_2$ + H $\rightarrow$ OH + OH	(108)
HO$_2$ + HO$_2$ $\rightarrow$ H$_2$O$_2$ + O$_2$	(109)
HO$_2$ + OH $\rightarrow$ H$_2$O + O$_2$	(110)
H$_2$O$_2$ + M $\rightarrow$ OH + OH + M	(112)
HO$_2$ + O $\rightarrow$ OH + O$_2$	(113)

On the other hand, the CO$_2$ formation in mixture A6 (fuel-rich condition) is very sensitive to the rate constants of reactions, 1, 3, 5, 9,16, 30, 35, 36, 52-54, 56, 62, 64, 68, 72, 84, 88-90, 94, 97, 98, 100, 101, 102, 107, and 164 as shown in Fig. 6b.

C$_2$H$_5$ (+ M) $\rightarrow$ C$_2$H$_4$ + H (+ M)	(- 16)
C$_2$H$_3$ + H $\rightarrow$ C$_2$H$_2$ + H$_2$	(30)

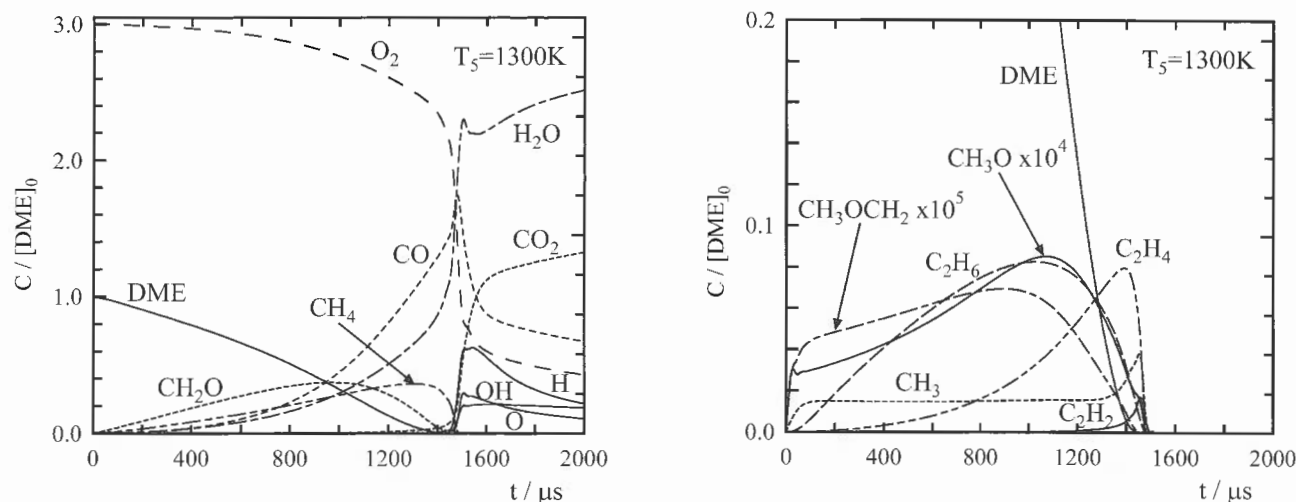Fig. 18. Species profiles for DME oxidation in stoichiometric DME-O_2-Ar mixture at T_5 = 1300 K, P_5 = 1.66 atm.

$C_2H_3 + O_2 \rightarrow CH_2CHO + O$	(35)
$C_2H_3 + CH_3 \rightarrow C_2H_2 + CH_4$	(36)
$CH_4 + H \rightarrow CH_3 + H_2$	(54)
$CH_4 + OH \rightarrow CH_3 + H_2O$	(56)
$CH_2 + O_2 \rightarrow CO_2 + H + H$	(72)
$CHO + H \rightarrow H_2 + CO$	(90)
$CHO + CH_3 \rightarrow CH_4 + CO$	(97)
$H_2 + O \rightarrow OH + H$	(101)
$H_2O + H \rightarrow OH + H_2$	(102)
$C_3H_6 \rightarrow C_2H_3 + CH_3$	(164)

4.10. Flow Diagram for the Dimethyl Ether Oxidation and Computed Profiles

Figure 17 presents the main oxidation routes of DME in stoichiometric DME-O_2-Ar mixture. At 1300 K, 1.66 atm and 800 μs, about 14 % of DME decomposes and produces CH_3 and CH_3O, about 71 % of DME reacts with H, O, OH and forms CH_3OCH_2 radicals and H_2, OH and H_2O, and about 14 % of DME reacts with CH_3 and gives CH_4 and CH_3OCH_2 radical. The formed CH_4 is rapidly consumed about 1400 μs later and generates CH_3, as seen in Fig. 18. The produced CH_3OCH_2 radical forms CH_3 and CH_2O. About 29 % of CH_3 produced forms CH_3O and about 30 % of CH_3 forms C_2H_6.

4.11. Application for Shock Tube Data at Low Temperature and High Pressure

To interpret data obtained at low temperatures (700 - 1100 K) and high pressures (13 and 40 atm) [5], our high temperature mechanism (DMEH-mec) were connected with the mechanism reported for low temperatures [3] (Table 2). For the calculation of 13 and 40 atm data, the rate constants

$k_1 = 1.62 \times 10^{41} T^{-7.46} \exp(-92.48 \text{ kcal/RT}) \text{ s}^{-1}$ (13 atm) and $k_1 = 1.45 \times 10^{34} T^{-5.3} \exp(-89.44 \text{ kcal/RT}) \text{ s}^{-1}$ (40 atm) of reaction 1 were used [3], respectively. This connected mechanism predicts well the ignition delays of stoichiometric DME and air mixture in the shock tube [5], as shown in Fig. 19. At low temperatures (700 - 1100 K) and high pressures (13 and 40 atm), reaction 2 is an important as the initiation reaction; our experimental data obtained at high temperatures (1100 - 1900 K) and low pressures (0.8 - 2.9 atm) is not sensitive to the rate constant of reaction 2. The consumption of DME was also sensitive to the rate constants of reactions 3, 5 - 8, 185, 186, 193 and 194; our experimental data obtained at high temperatures (1100 - 1900 K) and low pressures (0.8 - 2.9 atm) is not sensitive to the rate constants of reactions 6, 8, 179 - 195 and 196. Reactions 3, 5 - 8, 185, 186, 193 and 194 are particularly important at low temperatures (700 - 1100 K) and high pressures (13 and 40 atm).

DME is mainly consumed by reactions 3, 5, 6, 7 and - 182, especially 5, and produces the CH_3OCH_2 radical. The produced CH_3OCH_2 radical is mainly consumed by reactions 8 and 185, and produces CH_3 radical, $CH_3OCH_2O_2$ radical and CH_2O. $CH_3OCH_2O_2$ radical produces $CH_2OCH_2O_2H$ radical by reaction 191. $CH_2OCH_2O_2H$ radical produces CH_2O and OH radical by reaction 192.

4.12. Calculation with the Reported Mechanism

More recently, Fischer et al. [4] developed the new DME oxidation mechanism (FDC-mec) from data obtained with two different flow reactors, (1) a variable-pressure flow reactor at 2.5 atm and 1118 K, and (2) an atmospheric pressure flow reactor at about 1085 K; the mechanism consisted of 82 chemical species and 351 chemical reactions. The FDC-mec was applied for simulation of our observed

Table 2. Elementary Reactions and Rate Constant Expressions[a]

No.	Reaction	A	n	E_a	Reference
(1)	$CH_3OCH_3 = CH_3O + CH_3$	1.620E+41	-7.46	92480	3[b]
(1)	$CH_3OCH_3 = CH_3O + CH_3$	1.450E+34	-5.30	89440	3[c]
(179)	$CH_3OCH_3 + CH_3O_2 = CH_3OCH_2 + CH_3O_2H$	1.680E+13	0.00	17690	3
(180)	$CH_3OCH_3 + CH_3O = CH_3OCH_2 + CH_3OH$	6.020E+11	0.00	4074	3
(181)	$CH_3OCH_2 + CH_3O = CH_3OCH_3 + CH_2O$	2.410E+13	0.00	0	3
(182)	$CH_3OCH_2 + CH_2O = CH_3OCH_3 + CHO$	5.490E+03	2.80	5862	3
(183)	$CH_3OCH_2 + CH_3CHO = CH_3OCH_3 + CH_3CO$	1.260E+12	0.00	8499	3
(184)	$CH_3OCH_2 + HO_2 = CH_3OCH_2O + OH$	9.000E+12	0.00	0	3
(185)	$CH_3OCH_2 + O_2 = CH_3OCH_2O_2$	2.000E+12	0.00	0	3
(186)	$CH_3OCH_2O_2 + CH_3OCH_3 = CH_3OCH_2O_2H + CH_3OCH_2$	5.000E+12	0.00	17690	3
(187)	$CH_3OCH_2O_2 + CH_2O = CH_3OCH_2O_2H + CHO$	1.000E+12	0.00	11670	3
(188)	$CH_3OCH_2O_2 + CH_3CHO = CH_3OCH_2O_2H + CH_3CO$	2.800E+12	0.00	13600	3
(189)	$CH_3OCH_2O + OH = CH_3OCH_2O_2H$	2.000E+13	0.00	0	3
(190)	$CH_3O + CH_2O = CH_3OCH_2O$	1.000E+11	0.00	11900	3
(191)	$CH_3OCH_2O_2 = CH_2OCH_2O_2H$	6.000E+11	0.00	21580	3
(192)	$CH_2OCH_2O_2H = CH_2O + CH_2O + OH$	1.500E+13	0.00	20760	3
(193)	$CH_2OCH_2O_2H + O_2 = O_2CH_2OCH_2O_2H$	7.000E+11	0.00	0	3
(194)	$O_2CH_2OCH_2O_2H = HO_2CH_2OCHO + OH$	4.000E+10	0.00	18580	3
(195)	$HO_2CH_2OCHO = OCH_2OCHO + OH$	2.000E+16	0.00	40500	3
(196)	$CH_2O + HCO_2 = OCH_2OCHO$	1.250E+11	0.00	11900	3

[a] Rate constants in the form, $AT^n \exp(-Ea/RT)$, in cm, mol, cal, and K units.

[b] 10 atm

[c] 40 atm

CO_2 profiles. Comparison of the observed CO_2 profiles with those calculated using the FDC-mec is shown in Figs. 6a, 7 and 8a. The FDC-mec can reproduce well our fuel lean profiles (Fig. 8a), higher temperature profiles of fuel rich and stoichiometric mixtures (Figs. 6a and 7), but do not reproduce our lower temperature profiles of fuel rich and stoichiometric ones (Figs. 6a and 7).

5. Conclusion

New experimental data for the pyrolysis and oxidation of DME at high temperatures have been obtained from shock tube experiments using the following methods: 1) time-resolved IR-laser absorption at 3.39 μm for DME decay and CH-compound formation rates, 2) time-resolved UV absorption at 216 nm for CH_3 radical formation rate, 3) time-resolved UV absorption at 306.7 nm for OH radical formation rate, 4) time-resolved IR emission at 4.24 μm for CO_2 formation rate, and 5) a single-pulse technique for product yields. The DME pyrolysis and oxidation data, which were for mixture compositions ranging from DME-high rich (including DME pyrolysis) to DME- high lean, were modeled using a reaction mechanism with 178 reaction steps and 53 species including the most recent sub-mechanisms for formaldehyde, ketene, methane, acetylene, and ethylene oxidation. The rate constants of the reactions DME + OH $\rightarrow$ $CH_3OCH_2 + H_2O$ was evaluated.
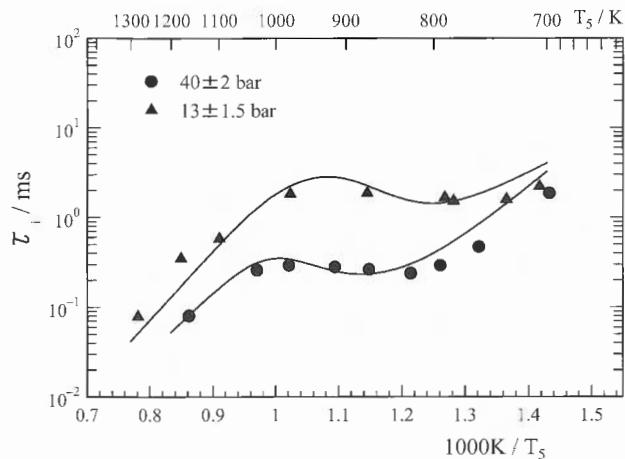
Fig. 19. Comparison of ignition delay times reported by Pfahl et al. [5] with those calculated.

References

1. Dagaut, P., Boettner, J. C., and Cathonnet, M., Twenty-sixth Symposium (International) on Combustion, *The Combustion Institute,* Pittsburgh, 1996, pp.627-632.

2. Dagaut, P., Daly, C., Simmie, J. M., and Cathonnet, M., Twenty-seventh Symposium (International) on Combustion, *The Combustion Institute,* Pittsburgh, 1998, pp.361-369.

3. Curran, H. J., Pitz, W. J., Westbrook, C. K., Dagaut, P., Boettner, J. C., and Cathonnet, M., *Int. J. Chem. Kinet.* 30: 229-241 (1998).

4. Fischer, S. L., Dryer, F. L., and Curran, H. J., *Int. J. Chem. Kinet.* 32:713-740 (2000).

5. Pfahl, U. Fieweger, K., and Adomeit, G., Twenty-sixth Symposium (International) on Combustion, *The Combustion Institute,* Pittsburgh, 1996, pp.781-789.

6. Hidaka, Y., Shiba, S., Takuma, H.,and Suga, M., *Int. J. Chem. Kinet.* 17: 441-453 (1985).

7. Hidaka, Y., Nakamura, T., Miyauchi, A., Shiraishi, T., and Kawano, H., *Int. J. Chem. Kinet.* 21: 643-666 (1989).

8. Hidaka, Y., Hattori, K., Okuno, T., Inami, K., Abe, T., and Koike, T., *Combust. Flame,* 107: 401-417 (1996).

9. Hidaka, Y., Kimura, K., Hattori, K., and Okuno, T., *Combust. Flame,* 106: 155-167 (1996).

10. Hidaka, Y., Taniguchi, T., Tanaka, H., Kamesawa, T., Inami, K., and Kawano, H., *Combust. Flame,* 92: 365-376 (1993).

11. Hidaka, Y., Higashihara, T., Nishimori, T., Sato, K., Henmi, Y., Okuda, R., and Inami, K., *Combust. Flame,* 117: 755-776 (1999).

12. Hidaka, Y., Higashihara, T., Ninomiya, N., Oshita, H., and Kawano, H., *J. Phys. Chem.* 97: 10977-10983 (1993).

13. Hidaka, Y., Taniguchi, T., Kamesawa, T., Masaoka, H., Inami, K., and Kawano, H., *Int. J. Chem. Kinet.* 25: 305-322 (1993).

14. Hidaka, Y., Takuma, H., and Suga, M., *Bull. Chem. Soc. Jpn.* 58: 2911-2916 (1985).

15. Hidaka, Y., Takahashi, S., Kawano, H., and Suga, M., and Gardiner, W. C., Jr., *J. Phys. Chem.* 86: 1429-1433 (1982).

16. Hidaka, Y., Higashihara, T., Ninomiya, N., Masaoka, H., Nakamura,T., and Kawano, H., *Int. J. Chem. Kinet.* 28: 137-151 (1996).

17. Hidaka,Y., Sato,K., Henmi,Y., Tanaka,H., and Inami, K., *Combust. Flame,* 118: 340-358 (1999).

18. Chase, Jr., et al., in JANAF Thermochemical Tables, 3rd ed., *J. Phys. Chem. Ref. Data,* Vol 14, Suppl. 1, 1985.

19. http://www.me.berkeley.edu/gri_mech/.

20. Hidaka, Y, Sato, K., and Yamane, M., *Combust. Flame* 123: 1-22 (2000).

21. Hidaka,Y., Sato,K., Henmi,Y., Tanaka,H., and Inami, K., *Combust. Flame* 118: 340-358 (1999).

22. Hidaka, Y., Sato, K., Hoshikawa, H., Nishimori, T., Takahashi, R., Tanaka, H., Inami, K., and Ito, N., *Combust. Flame* 120: 245-264 (2000).

23. Faubel, C., Hoyermann, K., Strofer, E., and Wagner, H. Gg., *Ber. Bunsenges. Phys. Chem.* 83: 532-538 (1979).

24. Lee, J. H., Machen, R. C., Nava, D. F., and Stief, L. J., *J. Chem. Phys.* 74: 2839-2844 (1981).

25. Marcus, R. A., Darwent, B. de B., and Steacie, E. W. R., *J. Chem. Phys.* 16: 987-991 (1948)

26. Trotman-Dickenson, A. F., and Steacie, E. W. R., *J. Chem. Phys.* 19: 329-334 (1951).

27. Loucks, L. F., *Can. J. Chem.* 45: 2775-2779 (1967).

28. Pacey, P. D., *Can. J. Chem.* 53: 2742-2747 (1975).

29. Held, A. M., Manthorne, K. C., Pacey, P. D., and Reinholdt, H. P., *Can. J. Chem.* 55: 4128-4134 (1977).

30. Gardiner, W. C., Jr., *J. Phys. Chem.* 81: 2367-2371 (1977).

31. Tsang, W., and Hampson R. F., *J. Phys. Chem. Ref. Data* 15: 1087-1279 (1986).

32. Sato, K., and Hidaka, Y., *Combust. Flame* 122: 291-311 (2000).

33. Hidaka, Y., Higashihara, T., Ninomiya, N., Oki, T., and Kawano, H., *Int. J. Chem. Kinet.* 27: 331-341 (1995).

34. Hidaka, Y., Masaoka, H., Oshita, H., Nakamura, T.,Tanaka, and Kawano, H., *Int. J. Chem. Kinet.* 24: 871-885 (1992).

35. Hidaka, Y., Nakamura, T.,Tanaka, H., Jinno, A., and Kawano, H., *Int. J. Chem. Kinet.* 24: 761-780 (1992).